

Viscoelastic interphases in polymer–matrix composites: theoretical models and finite-element analysis

F.T. Fisher, L.C. Brinson *

Department of Mechanical Engineering, Northwestern University, 2145 Sheridan Road, Evanston, IL 60208, USA

Received 21 January 2000; received in revised form 7 December 2000; accepted 18 January 2001

Abstract

We investigate the mechanical property predictions for a three-phase viscoelastic (VE) composite by the use of two micro-mechanical models: the original Mori–Tanaka (MT) method and an extension of the Mori–Tanaka solution developed by Benveniste to treat fibers with interphase regions. These micro-mechanical solutions were compared to a suitable finite-element analysis, which provided the benchmark numerical results for a periodic array of inclusions. Several case studies compare the composite moduli predicted by each of these methods, highlighting the role of the interphase. We show that the MT method, in general, provides the better micromechanical approximation of the viscoelastic behavior of the composite; however, the micromechanical methods only provide an order-of-magnitude approximation for the effective moduli. Finally, these methods were used to study the physical aging of a viscoelastic composite. The results imply that the existence of an interphase region, with viscoelastic moduli different from those of the bulk matrix, is not responsible for the difference in the shift rates, μ_{22} and μ_{66} , describing the transverse Young's axial shear moduli, found experimentally. © 2001 Published by Elsevier Science Ltd. All rights reserved.

Keywords: Interphase; Micromechanics; Viscoelasticity; Finite element analysis; Physical aging

1. Introduction

Polymer–matrix composites (PMCs), particularly those containing fiber reinforcement, have become increasingly popular for use in structural applications. The primary benefit of such systems is the potential for impressive strength-to-weight ratios. Other additional benefits, such as improved corrosion resistance and material property tailorability, can be of significance for specialized applications. One area of complication in the analysis of PMCs is the existence of an interphase region of finite dimensions. For PMCs, interphase weight fractions on the order of 5% of the total weight of the composite have been estimated experimentally [1]. In this case, one may expect the interphase region to influence the overall effective behavior of the composite. The goal of this work is to extend micromechanical solutions, developed for multiphase elastic materials, so that an analysis of a

PMC with a viscoelastic interphase may be undertaken. Such analytical models may be used to study the interphase region as related to:

1. modeling the effective behavior of composite materials,
2. optimizing composite properties through engineered interphases,
3. measuring the interphase mechanical properties through experimental tests,
4. more complex composite behavior (aging, damage, moisture absorption, etc.).

A review of the literature produces a large number of models developed for the prediction of the elastic moduli of composite materials. Excellent review articles are provided by Hashin [2] and Christensen [3]. Several researchers have used the Mori–Tanaka method to study multiphase composite behavior [4–6]. Other micro-mechanical analyses of effective composite behavior can also be found [7–9]. Weng [10] noted the relationship between the MT method and the Hashin–Shtrikman–Walpole bounds for multiphase elastic composites when the matrix is the stiffest or the softest elastic material.

* Corresponding author. Tel.: +1-847-467-2347; fax: +1-847-491-3915.

E-mail address: cbrinson@northwestern.edu (L.C. Brinson).

Analysis of viscoelastic composites using micro-mechanical techniques is less developed. Early work in this area was pioneered by Hashin [11–14] and Schapery [15,16]. Some researchers have looked at the effect of inclusion shape on the mechanical properties of two-phase VE composites [17,18]. Brinson and Lin [19,20] have compared the MT method with a finite-element analysis of two-phase VE composites. In the present work, two micromechanical methods and a finite-element solution will be used to analyze composites with VE interphases. As described in the next section, the correspondence principle is used to extend these solutions for viscoelastic materials.

The first micromechanical method used in this work is the Mori–Tanaka method [21–23]. The MT method has been used for a wide range of problems and thus become a popular tool for analysis of multiphase materials. Here we extend the model to study a three-phase fibrous composite consisting of isotropic, viscoelastic phase materials. As used here, the MT method does not model the geometry of an annular interphase region surrounding the fiber inclusion, but rather treats the fiber and interphase regions as separate, physically distinct regions as shown in Fig. 1. Although this approach at first glance may appear inappropriate for representing the real fiber-interphase-matrix geometry (see Fig. 2), the MT technique is so widely used and simple to employ that it is useful to know how accurate the prediction may be in this context.

The second micromechanical solution follows the model proposed by Benveniste et al. [24] to study materials with coated inclusions. This model maintains the proper fiber-interphase-matrix geometry as shown in Fig. 2. It utilizes a related auxiliary problem (i.e. a single fiber-interphase inclusion within an infinite matrix material) to find the stress-concentration tensors relating an applied far-field stress to the phase-averaged stresses of the included (fiber and interphase) phases. Assuming

that these tensors remain valid for the related, multiple-inclusion composite (where the stress which the inclusions now “feel” is the unknown average matrix stress), the overall composite moduli can be determined.

For comparison, a finite element analysis with the included phases aligned in an hexagonal array was also completed. We use the dynamic correspondence principle to solve the unit cell boundary value problem necessary to obtain the effective complex moduli of the composite [25]. A hexagonal array of inclusions yields transversely isotropic composite behavior, allowing direct comparison between the FEA and micromechanical solutions. Other researchers have used alternative interface/interphase models to study the interaction between the fiber and matrix regions [26–28], as well as FEA to study the effective moduli of composites with elastic interphases [29–31]. Yi et al. [32] found that for composites with viscoelastic interphases, the effective transverse modulus was largely dependent on the volume fraction of the fiber and the viscoelastic behavior of the matrix.

The following section provides background information concerning viscoelasticity, the correspondence principle, and the role of the interphase for PMCs. The extension of the micromechanical methods and the FEA for viscoelastic materials will then be briefly outlined, after which the results of the models will be presented and discussed. Finally, these models will be used to investigate the impact of a viscoelastic interphase on the physical aging of polymer matrix composites.

2. Background

In this paper, we analyze the mechanical response of a fiber-reinforced polymer matrix composite with a viscoelastic interphase region. Recent experimental evidence suggests that the interphase region could be larger than previously believed, making it necessary to explicitly

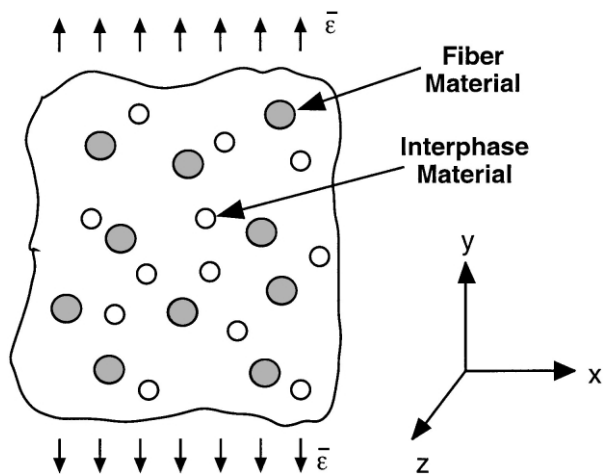


Fig. 1. Interphase modeled as a distinct inclusion region for the Mori–Tanaka method.

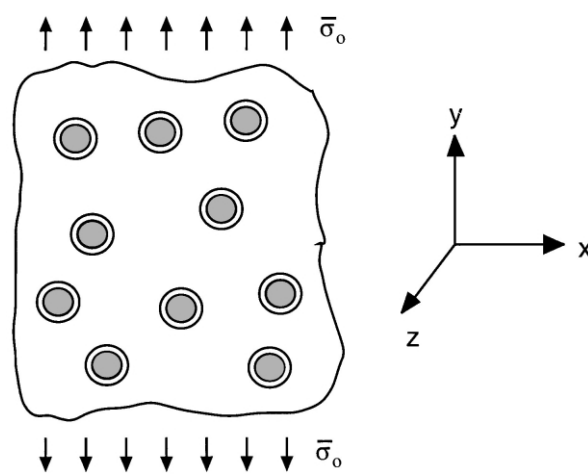


Fig. 2. Three phase composite model for the Benveniste solution. a = Radius of fiber; b = outer radius of interphase.

account for such a region from a design perspective. Properties of the interphase region can be expected to differ from the other bulk materials [33]. Because analysis of the time-dependent response with VE phase materials can become computationally prohibitive, the dynamic correspondence principle is used to study the associated problem in the frequency domain. Two hypothetical VE materials, and a hypothetical elastic fiber, are used for the numerical simulations presented in this paper.

2.1. The interphase region

The interphase (or mesophase) refers to the inhomogeneous region surrounding the inclusions in a composite material. Interphase regions may be due to voids, mechanical imperfections, unreacted polymer components, fiber treatments, restricted macromolecular mobility due to the fiber surface, and other inconsistencies [34–36]. In addition, there are “engineered interphases”: the deliberate introduction of a novel third phase (for example, fiber sizings), with mechanical properties on the order of magnitude of the matrix, to optimize composite performance. In each case, a relatively small volume fraction of interphase may play a crucial role in determining the overall mechanical response of the composite.

One difficulty that is encountered when modeling the interphase is the characterization of the size and properties of the region. Experimental work to better determine these parameters are ongoing. In the past, the thickness of a PMC interphase has been estimated to be between 30 and 240 nm [37], and similar results were reported in an experimental study using scanning force microscopy [38]. However, other recent experimental findings suggest that the interphase region within PMC materials may be larger. These techniques, including secondary ion mass spectroscopy [1] and atomic force microscopy [39], suggest interphase thicknesses on the order of 1 μm for glass-fiber epoxy composites. An example of PMC interphase thicknesses measured experimentally are summarized in Table 1.

Another atomic force microscopy study [40] showed that variations in the fiber sizing can impact the creation of the interphase region. In this study, the matrix material was unable to completely diffuse into a thick fiber sizing, and hence a distinct interphase region was realized. For a thinner fiber sizing, the matrix was able to

diffuse into the fiber sizing such that no discernible interphase could be detected. Obviously, a better understanding of the interphase region will be necessary as models to predict the behavior of composites with finite interphase regions are developed. In this paper, a nominal interphase area fraction of 10% was used (unless otherwise noted) to maximize the influence of the interphase on the effective moduli of the composite.

2.2. Viscoelasticity and the correspondence principle

The constitutive equation for a viscoelastic material can be written in terms of a Stieltjes integral equation of the form

$$\sigma_{ij}(t) = \int_{-\infty}^t C_{ijkl}(t - \xi) \frac{d\varepsilon_{kl}(\xi)}{d\xi} d\xi, \quad (1)$$

where σ_{ij} and ε_{kl} are standard stress and strain tensors and C_{ijkl} is the time-dependent modulus. For isotropic VE materials, the mechanical response can be characterized by the time-dependent bulk and shear moduli, $K(t)$ and $G(t)$, respectively. However, it is possible to completely avoid time domain analysis by utilizing the *dynamic correspondence principle*, where the mechanical characterization of viscoelastic materials is completed in the transformed (frequency) domain [11]. This is accomplished by considering a separable form for the displacements,

$$u_i(\mathbf{x}, t) = \bar{u}_i(\mathbf{x}, \omega) e^{i\omega t}, \quad (2)$$

where ω is frequency, \mathbf{x} is position, and transformed quantities are denoted by an overbar. Given (2), the constitutive equations for an isotropic viscoelastic material can be written in terms of transformed deviatoric and dilatational stress components,

$$\bar{s}_{ij} = 2 \bar{G}^*(\omega) \bar{\varepsilon}_{ij}, \quad \bar{\sigma}_{kk} = 3 \bar{K}^*(\omega) \bar{\varepsilon}_{kk}, \quad (3)$$

where the complex bulk and shear moduli, $\bar{K}^*(\omega)$ and $\bar{G}^*(\omega)$, are defined as

$$\begin{aligned} \bar{K}^*(\omega) &\equiv i\omega \bar{K}(\omega) = i\omega \int_0^\infty K(t) e^{-i\omega t} dt; \\ \bar{G}^*(\omega) &\equiv i\omega \bar{G}(\omega) = i\omega \int_0^\infty G(t) e^{-i\omega t} dt. \end{aligned} \quad (4)$$

Table 1
Experimental interphase thicknesses for PMC materials

Researcher	Year	Method	Thickness	Material
Theocarlis [36]	1985	Differential scanning calorimetry	30–240 nm	Glass-fiber/epoxy $v_f=10\text{--}70\%$
Thomason [1]	1995	Secondary ion mass spectroscopy	1 μm	Glass-fiber/epoxy $v_f=65\%$; $d_f=25\ \mu\text{m}$
Munz et al. [38]	1998	Scanning force microscopy	75–150 nm	Carbon-fiber/poly-phenylenesulfide
Mai et al. [39]	1998	Atomic force microscopy	1–3 μm	Carbon-fiber/epoxy single fiber

These complex moduli are typically written in terms of the storage and loss moduli,

$$\begin{aligned}\bar{K}^*(\omega) &= K'(\omega) + iK''(\omega), \\ \bar{G}^*(\omega) &= G'(\omega) + iG''(\omega),\end{aligned}\quad (5)$$

where single and double primes denote the storage and loss moduli, respectively. The storage modulus is a measure of the elastic response of the material, whereas the loss moduli represents viscous (damping) behavior [41].

Note that the constitutive equations in (3) are analogous to the standard elasticity formulation, where now all field quantities are complex. Thus, there is a direct relationship between elasticity problems in the time domain and viscoelasticity problems in the frequency domain. We take advantage of this relationship by transforming appropriate elasticity solutions into the frequency domain and replacing the elastic moduli with the related complex moduli defined in (4). The response of the composite can be found by completing the desired analysis for an appropriate range of frequencies.

2.3. Constituent materials

Our goal is to determine the effective moduli of a three phase viscoelastic composite consisting of cylindrical fibers, surrounded by an annular interphase, and embedded in a binding, continuous matrix. Perfect bonding between the phases is assumed. Both the matrix and interphase are isotropic, linear viscoelastic materials, whereas the fiber is isotropic elastic. Temperature effects were not studied in the first part of this work, although the physical aging study presented at the end of this paper assumes an isothermal temperature below the glass transition temperatures (T_g) of each viscoelastic material. It should be noted that the T_g of the interphase may also vary significantly from the other viscoelastic phases of the composite. Processing temperatures greater than the interphase T_g will increase molecular mobility in the region, enhancing the ability of the interphase to properly bond with the other constituent materials [1].

For this investigation two hypothetical viscoelastic materials, designated “stiff” and “soft”, were used as the matrix and interphase materials in a three-phase composite. Various area fractions and permutations of the constitutive materials were analyzed. The viscoelastic bulk and shear moduli of these two materials were represented using a standard Prony series representation of the form

$$A(t) = A_\infty + \sum_{j=1}^N A_j e^{-t/\tau_j}, \quad (6)$$

where A_j and τ_j represent the relaxation spectra and relaxation times, respectively, and A_∞ is the rubbery asymptotic value of the appropriate modulus. The parameters used to obtain the viscoelastic behavior of the “stiff” and “soft” materials are given in Table 2. The fiber, always the stiffest of the three phases, had elastic moduli characterized by $G_f = 40,000$ and $K_f = 100,000$.¹

3. Micro-mechanical methods

Two micro-mechanical analyzes, the original Mori–Tanaka method and an extension of this solution proposed by Benveniste, are used to predict the mechanical behavior of a three-phase composite. The former is a standard micromechanical tool which only approximates the composite geometry, whereas the latter keeps the physicality of an annular interphase region intact. Because the micromechanical solutions are easier to implement than a full FEA, it will be useful to ascertain the ability of these methods to provide approximations of the composite response.

3.1. Mori–Tanaka method

The formulation of the Mori–Tanaka method for the determination of the effective moduli of a viscoelastic composite is briefly presented. More detailed derivations can be found in the literature [21–23]. As used here, the MT method approximates the fiber-interphase problem using a composite with distinct cylindrical inclusions representing the fiber and interphase regions (see Fig. 1). Since the Mori–Tanaka method is a standard micromechanical tool and easy to apply, it will be valuable to determine the approximate solution the Mori–Tanaka method provides in this context.

The individual phases which comprise the composite are denoted f , g , and m for the fiber, interphase, and matrix, respectively. Area fractions for each phase are denoted c_k , where $k = \{f, g, m\}$, a is the fiber radius, and b is the outer radius of the interphase; thus,

$$c_f = \pi a^2; \quad c_g = \pi(b^2 - a^2); \quad c_m = 1 - c_f - c_g. \quad (7)$$

Following the standard elastic derivation, and implementing the correspondence principle to account for viscoelasticity, one can show

¹ While unitless parameters are used here, the *ratios* of the constituent moduli (e.g. fiber to matrix) are consistent with those used by other researchers for finite element analyzes of polymer matrix materials [29] and representative of common composite constituent materials.

Table 2
Prony series terms for the viscoelastic moduli of the “stiff” and “soft” hypothetical materials

Stiff material		Soft material	
$G_\infty = 100$		$G_\infty = 3.162$	
$K_\infty = 8000$		$K_\infty = 200$	
τ_j^G	G_j	τ_j^G	G_j
3.0	3.162	0.032	2.512
10.0	17.783	0.100	10.0
32.0	100.0	0.316	56.234
100.0	316.228	1.0	316.228
316.0	1000.0	3.162	1000.0
1000.0	5623.413	10.0	199.526
3162.0	10000.0	31.623	50.119
10000.0	562.341	100.0	19.953
31623.0	141.254	316.228	12.589
100000.0	56.234	1000.0	2.512
316228.0	17.783	3162.278	1.698
1000000.0	5.623	10000.0	1.202
3162278.0	3.162	31622.777	1.148
10000000.0	1.778	100000.0	1.096
τ_j^K	K_i	τ_j^K	K_i
10000	40000	100	3000
		316.228	100

$$\left[\bar{\mathbf{S}}_k^* + \frac{\bar{\mathbf{L}}_m^*}{\bar{\mathbf{L}}_k^* - \bar{\mathbf{L}}_m^*} \right] \bar{\mathbf{A}}_k - \sum_n c_n \bar{\mathbf{S}}_n^* \bar{\mathbf{A}}_n = -\mathbf{I}, \quad (k, n = \{f, g\}), \tag{8}$$

where n is a dummy variable, $\bar{\mathbf{L}}_m^*$ is the complex stiffness of the matrix, $\bar{\mathbf{L}}_k^*$ and $\bar{\mathbf{S}}_k^*$ are the complex stiffness and the Eshelby tensor of the k th inclusion (evaluated using the complex matrix properties), and \mathbf{I} is the fourth-order identity tensor. The strain-concentration tensors $\bar{\mathbf{A}}_f$ and $\bar{\mathbf{A}}_g$ found via (8) relate the uniform applied strain $\bar{\boldsymbol{\epsilon}}$ to the transformation strain $\tilde{\boldsymbol{\epsilon}}_k^*$ of the included phases via the relationship $\tilde{\boldsymbol{\epsilon}}_k^* = \bar{\mathbf{A}}_k \bar{\boldsymbol{\epsilon}}$. The effective modulus of the composite, $\bar{\mathbf{L}}^*$, is found to be

$$\bar{\mathbf{L}}^* = \bar{\mathbf{L}}_m^* \left[\mathbf{I} - \sum_k c_k \bar{\mathbf{A}}_k \right], \quad (k = \{f, g\}). \tag{9}$$

Once the effective complex stiffness of the composite has been determined, it is straightforward to determine five transversely isotropic material moduli that describe the mechanical response.

3.2. Benveniste solution

Benveniste et al. [24] have proposed a model to evaluate the effective moduli of a three phase elastic composite based on the local fields of composites with coated inclusions. This derivation explicitly considers an annu-

lar interphase, and as such models the actual geometry of the interphase region. The local stress fields in the fiber and interphase are approximated by those of an *auxiliary problem*, a *single* fiber-interphase inclusion embedded in an infinite medium of matrix material and subjected to an appropriate far-field stress field. The superposition of auxiliary problems necessary to determine the complex transverse Young’s modulus, \bar{E}_{22}^* , is shown in Fig. 3. Particle interaction is described through the unknown average matrix stress, in a manner identical to that used in the MT method. The effective moduli are found by considering different far-field loadings; the reader is referred to the original work of Benveniste for a complete derivation.

Using the correspondence principle to account for viscoelastic behavior, the displacements for each auxiliary problem can be written in terms of unknown complex constants. The analysis then proceeds along the lines of a standard elasticity solution in complex space by simply carrying through the complex variables. Thus, Hooke’s Law and the strain-displacement equations provide the analytic expressions for the stress and strain fields in each phase of the auxiliary problem. Enforcing suitable boundary conditions provides the complex displacement constants, allowing the phase-average stresses in each included phase to be determined. Appropriate stress-concentration tensors, $\bar{\mathbf{W}}^k$ for $k = \{f, g\}$, are then defined to relate the far-field applied stress of the auxiliary problem, $\bar{\boldsymbol{\sigma}}_o$, to the primary phase-average stress component of the included phases, $\bar{\boldsymbol{\sigma}}_{ij}^k$,

auxiliary problem

$$\bar{\boldsymbol{\sigma}}_{ij}^k = \bar{\mathbf{W}}^k \bar{\boldsymbol{\sigma}}_o. \quad (k = \{f, g\}). \tag{10}$$

Once these tensors have been determined for the auxiliary problem, it is assumed that they are also valid for the actual (multiple inclusion) composite geometry. In this case, the applied stress to which the included phases are subjected is the average matrix stress, such that

multiple inclusion geometry

$$\bar{\boldsymbol{\sigma}}_{ij}^k = \bar{\mathbf{W}}^k \bar{\boldsymbol{\sigma}}_{ij}^m. \quad (k = \{f, g\}) \tag{11}$$

One can now enforce consistency for the actual composite geometry, given the absence of body forces, to find the average matrix stress within the composite. Using (11), the primary phase-averaged stresses for all phases within the actual composite can be determined. Using these average stresses, the average strain within each phase can be determined; at this point it is then straightforward to determine the complex composite moduli. This procedure is further outlined in the appendices.

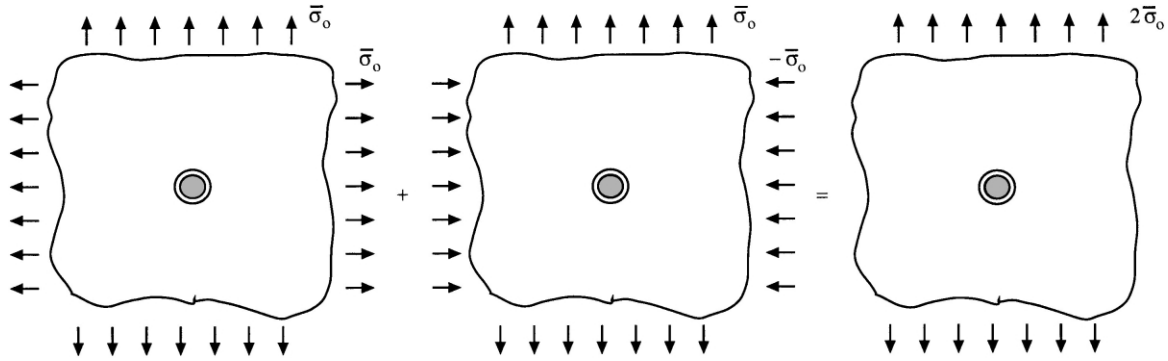


Fig. 3. Superposition of the transverse hydrostatic and transverse shear auxiliary problems for the determination of the transverse Young's modulus.

4. Finite element formulation

A two-dimensional finite element analysis (FEA) was undertaken on the unit cell models of Figs. 4 and 5. Plane strain conditions were assumed. The mesh was refined until a convergent solution for a hexagonal array of inclusions was found. These results were then used as the benchmark numerical result for transversely isotropic composite behavior. Although stress fields and related localized phenomena (such as plasticity and failure initiation) are very dependent on the inclusion arrangement, the effective moduli of composite materials are largely

independent of inclusion packing [31]. Therefore, the results of this section will provide a baseline by which the results of the two micromechanical methods may be judged, although neither analytical method explicitly represents a periodic array of inclusions. Because it is assumed that the reader is familiar with the finite element method for elastic materials, we will mention only briefly the modifications necessary for a viscoelastic boundary value problem. This finite element work follows that of Brinson and co-workers [19,25,42] for two phase viscoelastic materials. Suitable boundary conditions for the transverse Young's and transverse shear complex moduli, \bar{E}_{22}^* and \bar{G}_{44}^* , are given in Figs. 4 and 5.

For the transverse Young's modulus unit cell shown in Fig. 4, the top face is given a uniform displacement of \bar{u}_0 . The prescribed displacement $-\bar{b}$ at $x = W$ ensures that the right-hand side of the unit cell remains straight and parallel upon deformation. This displacement is chosen by simple interpolation such that the traction boundary condition at $x = W$ is approximated as

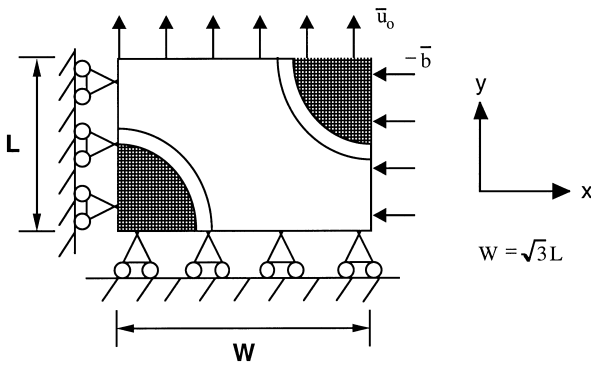


Fig. 4. Unit cell analysis to determine the complex transverse Young's modulus.

$$\int_0^L \bar{T}_x \, dy = 0, \quad \text{at } x = W \tag{12}$$

where \bar{T}_x are the resultant nodal tractions on the right hand side of the unit cell. Alternative methods to satisfy (12) are discussed in the literature [25]. The average resulting normal stress $\bar{\sigma}_{y,ave}(\omega)$ on the top face of the unit cell was obtained by summing the resultant nodal forces at $y = L$ and dividing by the area. Given the prescribed normal strain across the top face of the unit cell, $\bar{\epsilon}_y = \bar{u}_0/L$, the complex transverse Young's modulus of the composite can be determined via

$$\bar{E}_{22}^*(\omega) = i\omega \bar{E}_{22}(\omega) \equiv \frac{\bar{\sigma}_{y,ave}(\omega)}{\bar{\epsilon}_y} \tag{13}$$

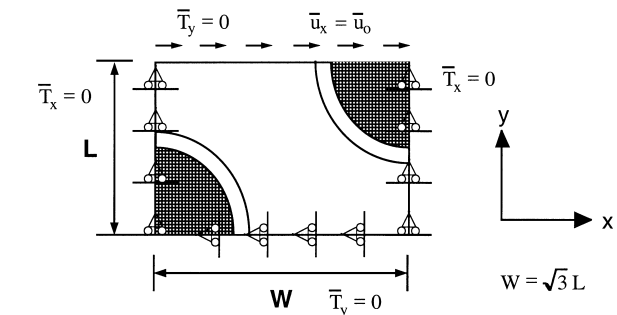


Fig. 5. Unit cell analysis to determine the complex transverse shear modulus.

A similar procedure is required to determine the complex transverse shear modulus of the composite (see Fig. 5). Solution of this problem does not require inter-

polation to provide suitable boundary conditions. Applying a uniform shear strain $\bar{\gamma}_{xy} \equiv \frac{u_0}{L}$ across the top face of the unit cell, one can show

$$\bar{G}_{44}^*(\omega) = i\omega \bar{G}_{44}(\omega) \equiv \frac{\bar{\sigma}_{xy,ave}(\omega)}{\bar{\gamma}_{xy}}, \quad (14)$$

where $\bar{\sigma}_{xy,ave}(\omega)$ is the sum of the resultant nodal forces along the top face of the unit cell in the x -direction divided by the width of the unit cell.

5. Results

The models discussed in the previous sections were used to predict composite moduli as a function of the properties and volume fractions of the constituent materials. These results will provide insight as to the ability of the analytical models to capture the mechanical behavior predicted by the more thorough FEA. The storage and loss components of the transverse Young’s modulus for a composite consisting of 30% elastic fiber, 10% stiff interphase, and 60% soft matrix are shown in Figures 6 and 7. Note that 60% fiber cases have also been examined [43] and show similar trends to those presented in this paper. Cases with 30% fiber and 10% interphase were chosen for illustration in order to emphasize the influence of the interphase on the viscoelastic moduli of the composite. Here again “stiff” or “soft” refer to the viscoelastic material moduli described earlier.

Also included in these figures are the transformed Reuss and Voigt bounds (i.e. the Rule of Mixtures). Note that in Fig. 7 loss moduli predictions appear to violate these bounds at intermediate frequencies. This apparent discrepancy is admissible because the transformed bounds are not in fact valid in the frequency domain. Schapery [16] notes that, for composites with isotropic phase materials, transformed bounds hold for the “operational moduli” (i.e. the transformed moduli in Laplace space) of the composite. Indeed, it was verified numerically that the micromechanical solutions and FEA results do fall within the bounds when the Laplace transform is used in the above formulations. Gibiansky and co-workers [44,45] have developed bounding methods in the Fourier domain for a limited number of moduli for two-phase viscoelastic composites.

Figs. 6 and 7 indicate that, for stiff-interphase composites, the micromechanical predictions for \bar{E}_{22}^* are in close agreement with both each other and the FEA results; this was found to be true for included phase area fractions (fiber plus interphase) approaching 70%. Since the results for \bar{G}_{44}^* are similar, a detailed discussion of these results will not be included. For comparison, the transverse moduli for the complementary composite configuration (30% elastic fiber, 10% soft interphase, 60% stiff matrix) are shown in Figs. 8 and 9. For soft-interphase composites, a large discrepancy was found to exist between the two micromechanical models, with the FEA results falling between these two methods. Comparing this behavior with that of the constituent phases (also shown in Figs. 8 and 9), we see that the frequency-dependence of the Benveniste solution is in general

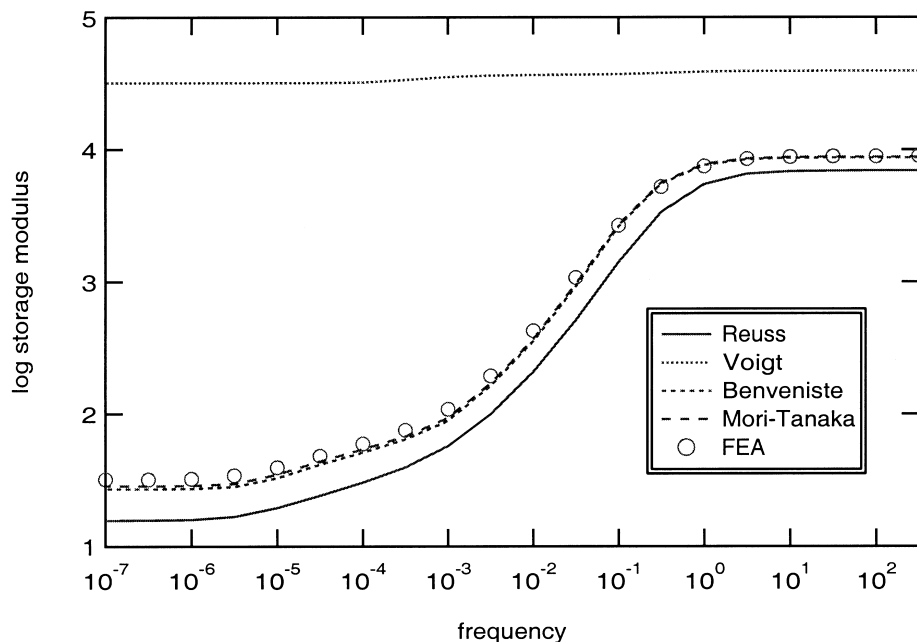


Fig. 6. Transverse Young’s storage moduli solutions for a composite with 30% elastic fiber, 10% stiff interphase, 60% soft matrix.

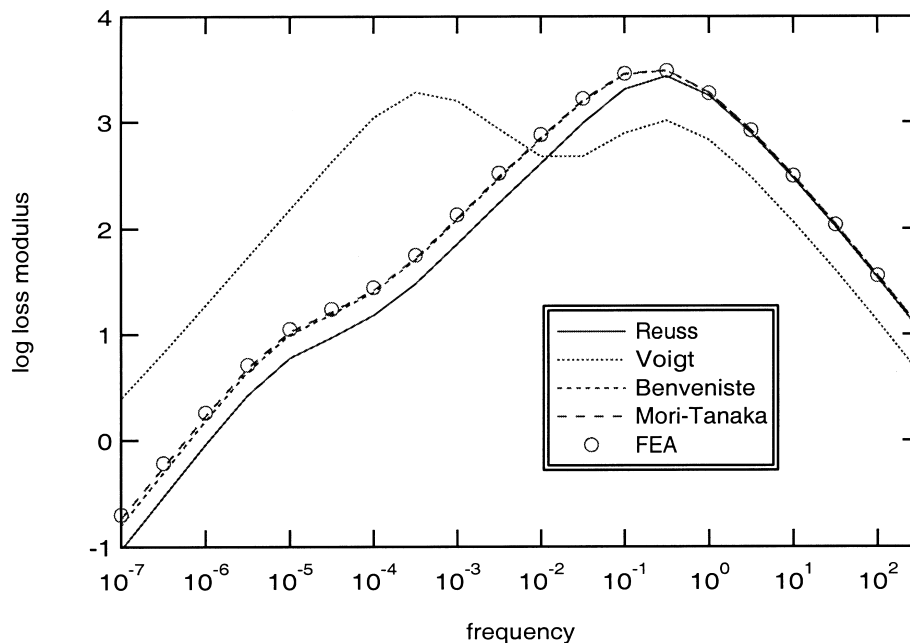


Fig. 7. Transverse Young's loss moduli solutions for a composite with 30% elastic fiber, 10% stiff interphase, 60% soft matrix.

dominated by the interphase material (most explicitly seen in the loss modulus), even though it is a non-continuous phase making up only a small portion of the composite. This result is viewed as a major drawback of the Benveniste solution, particularly for the analysis of the soft-interphase composites.

We believe that this flaw is largely due to the inability of the Benveniste solution to accurately model the influence of the interphase on the stress transfer between the fibers and matrix. This is illustrated in Fig. 10, where the normalized (with respect to the average matrix stress), phase-averaged real component of $\bar{\sigma}_{yy}$ as calculated via the FEA and the Benveniste solution are compared for the soft-interphase composite configuration discussed above. For this composite configuration, the Benveniste solution severely overestimates the average stress in the included phases at all frequencies. We believe this is caused by the smearing of the “phase-averaged” stresses required to determine the stress-concentration tensors necessary for this procedure. However, in the case of a stiff-interphase composite (not shown), the Benveniste solution is able to more closely model the stress transfer between the soft matrix and the fibers, which suggests use of the Benveniste model for stiff-interphase composites only [43].

Fig. 11 shows that the FEA predictions of the stress distribution for the two complementary composite configurations (soft interphase versus stiff interphase) are very different, and in both cases, far from uniform. This agrees with published experimental results for a three-phase epoxy matrix composite [31]. While Fig. 11 shows

results for a particular frequency within the transition region of the constituent materials ($\omega = 1E-4$), this was found to be true for all configurations and frequencies tested. It appears that micromechanical models which assume a uniform stress distribution within the constituent materials may be severely oversimplifying the analysis of the problem.

The Mori–Tanaka solution, even though it does not model the actual geometry of the problem, seems to better approximate the viscoelastic behavior of the moduli in that the effective moduli are dominated by the matrix material. Because the MT method treats the fiber and interphase as separate inclusions, the solution for soft interphase composites does not rely on the transfer of stress through the interphase. These conclusions and results are consistent with those obtained for other moduli and phase area fractions [43].

Figs. 12 and 13 show the components of \bar{E}_{22}^* as a function of interphase area fraction for a constant c_f of 30% and at fixed frequency of $1E-4$; this is within the transition region of each viscoelastic material. The results show that both micromechanical solutions provide very good approximations when the interphase is the stiff VE material, whereas the predictions are again poor when the interphase is the soft material. Again, these results were representative of others obtained for different composite configurations and at different frequencies. In the limit case of zero interphase area fraction, the micromechanical solutions are identical since both utilize the concept of an “unknown average matrix stress” to account for inclusion interaction. A comparison of the

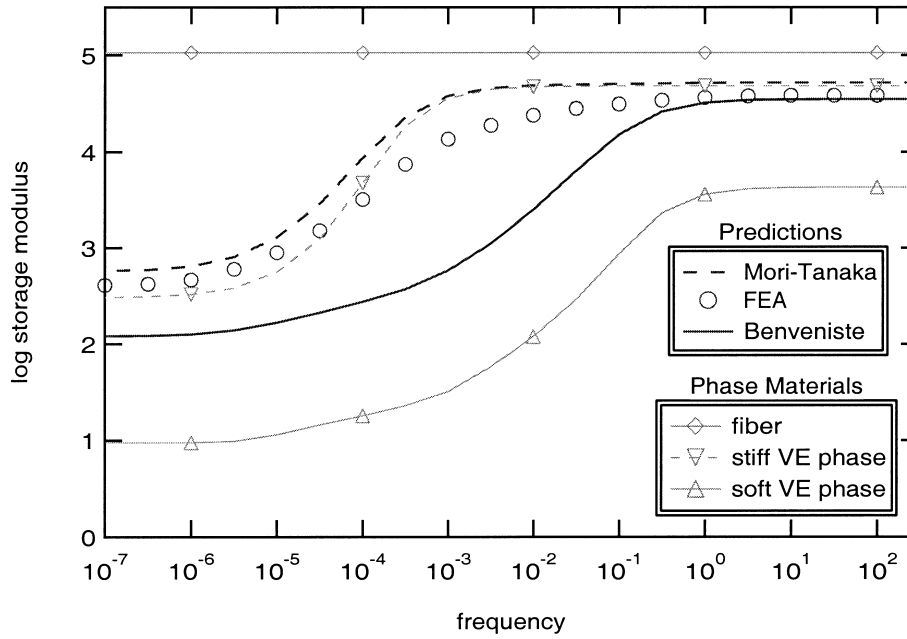


Fig. 8. Transverse Young’s storage moduli solutions for a composite with 30% elastic fiber, 10% soft interphase, 60% stiff matrix.

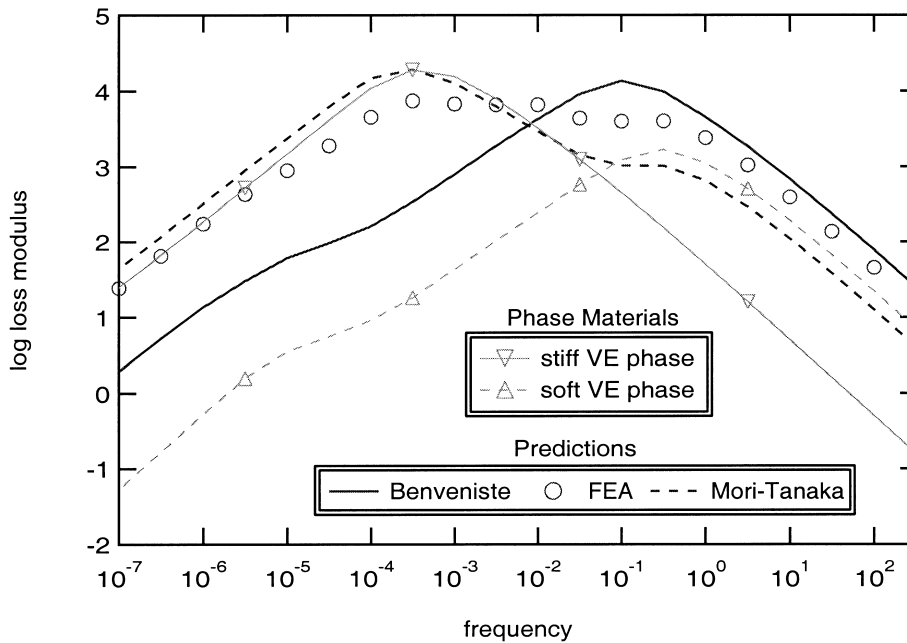


Fig. 9. Transverse Young’s loss moduli solutions for a composite with 30% elastic fiber, 10% soft interphase, 60% stiff matrix.

Mori–Tanaka method and a comparable finite element analysis for a two phase composite was presented in a previous study [19].

6. Physical aging case study

Physical aging has been the subject of numerous investigations; for an in-depth review of the subject see Ferry [41] and Struik [46]. Physical aging occurs because

a polymeric material below its glass transition temperature (T_g) is in a non-equilibrated thermodynamic state. As the polymer slowly approaches equilibrium, changes in mechanical behavior, and other phenomena, are realized. Similar to time-temperature superposition, the mechanical response at different aging times (t_e) can be superposed via a horizontal shifting of a master reference curve by an amount equal to the aging time shift factor (a_{t_e}). These shift factors are related to aging time via the shift rate μ ,

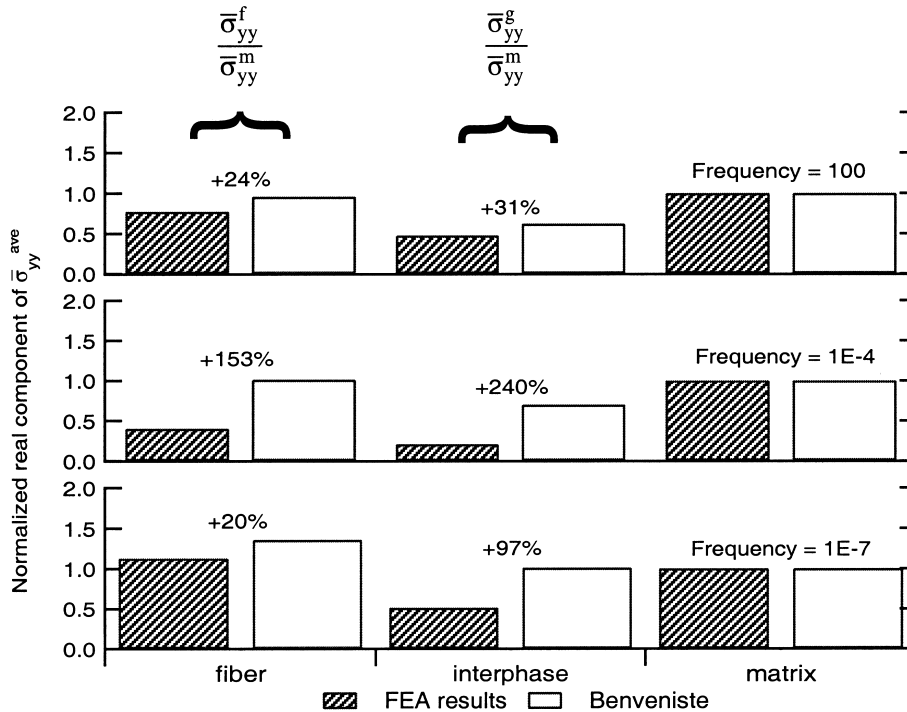


Fig. 10. Comparison of the phase-averaged real components of $\bar{\sigma}_{yy}^{ave}$ from the FEA and Benveniste solutions for a 30% elastic fiber, 10% soft interphase, 60% stiff matrix composite at three different frequencies (+xx% refers to the difference between the Benveniste solution and the FEA prediction).

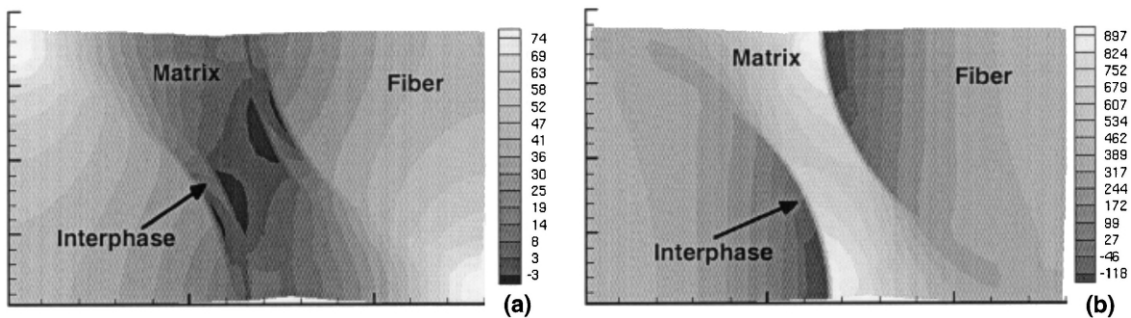


Fig. 11. Comparison of the σ_{yy}^{Re} stress distribution for transverse normal loading at a frequency of 1E-4 for 60% elastic fiber composites with (a) stiff interphase, (b) soft interphase.

$$\mu = -\frac{d \log a_{t_e}}{d \log t_e} \tag{15}$$

Struik [46] has demonstrated that the shift rates describing all mechanical properties for a homogeneous polymer are identical. However, experimental work on polymer matrix composites suggests that different shift rates, μ_{22} and μ_{66} , are required to characterize the physical aging of the transverse normal and axial shear responses, respectively; this despite the fact that both are considered matrix-dominated properties [47,48].

Here we investigate whether an interphase with aging properties distinct from those of the matrix could be responsible for the different shift rates measured experi-

mentally. It should be stressed that the investigation presented here is not rigorous; our 2D finite element code cannot determine the axial shear modulus of the composite. Instead we will analyze the aging behavior of the *transverse* shear modulus, another matrix-dominated property. Thus, the shift rates μ_{22} and $\mu_{44} = \mu_{55}$ will be analyzed via FEA to determine whether differences in matrix and interphase shift rates could be responsible for the distinct effective shift rates seen experimentally for PMCs.

Shift rates of 0.85 for the interphase and 0.70 for the matrix were assigned for all trials. FEA was then used to calculate \bar{E}_{22}^* and \bar{G}_{44}^* of the composite at different aging times. From the complex moduli, the time-dependent moduli, $E(t)$ and $G(t)$, could be determined using a

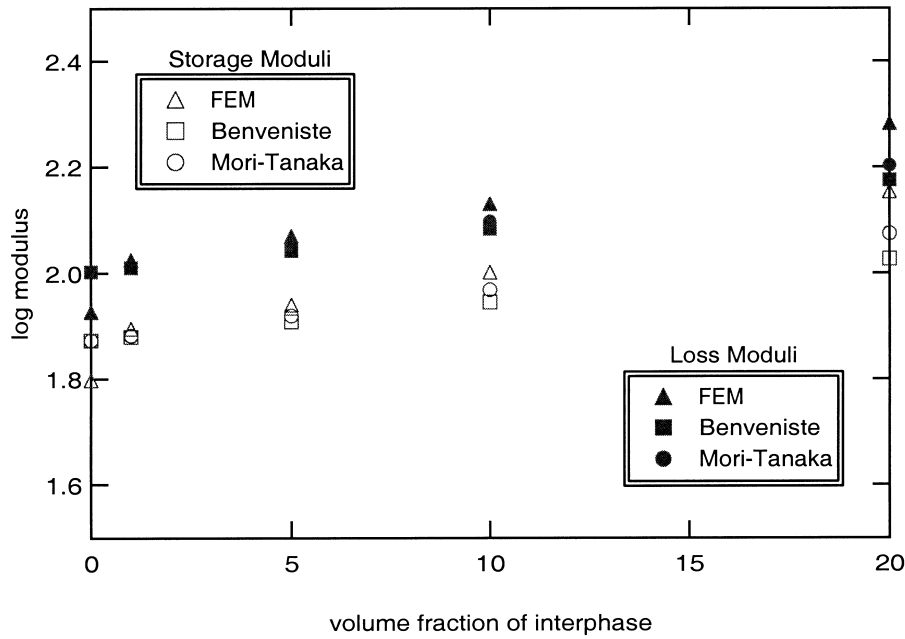


Fig. 12. Complex transverse Young's moduli versus interphase volume fraction for composites with 30% fiber, stiff interphase, and soft matrix material at a frequency of 1E-4.

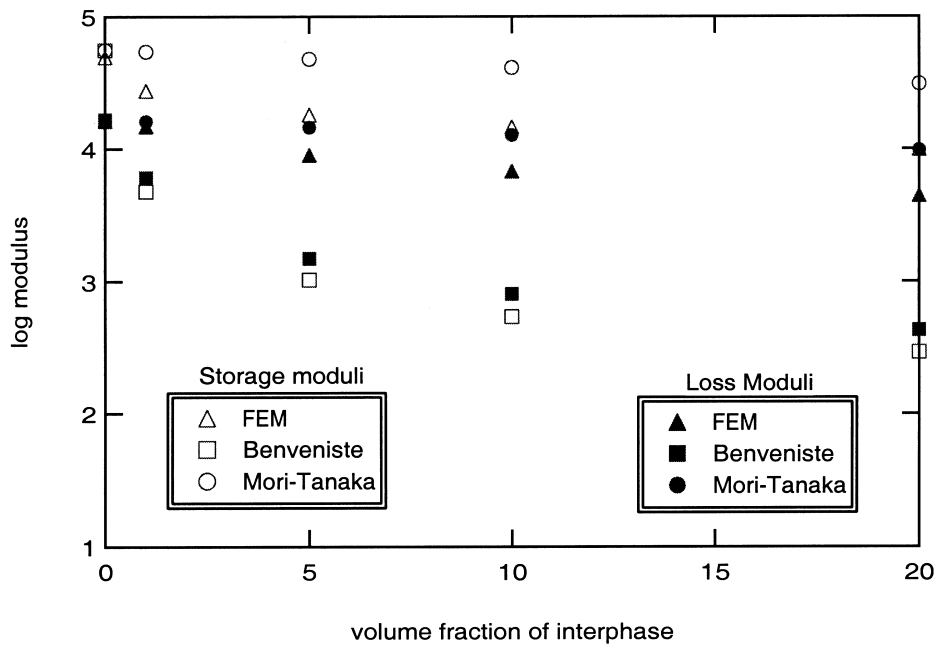


Fig. 13. Complex transverse Young's moduli versus interphase volume fraction for composites with 30% fiber, soft interphase, and stiff matrix material at a frequency of 1E-4.

linear least-squares solver [49]. Time-aging time superposition was performed on the different aged moduli to determine the shift rates of the composite for each of the two moduli. Note that shift rates can only be determined if the moduli functions at different aging times are superposable via a simple shift along the ordinate axis. This represents physical aging having an equal impact on all relaxation times describing the mechanical behavior.

Fig. 14 shows the frequency-dependent aging behavior of the transverse shear loss modulus for a soft-interphase composite as predicted by the finite element analysis. The reference curve in Fig. 14 (assigned as the initial aging time $t_{age} = 1$) has been shifted so as to best coincide with the moduli curves at other aging times. Note that while the reference curve has been shifted to superpose low frequency data, the high frequency ends

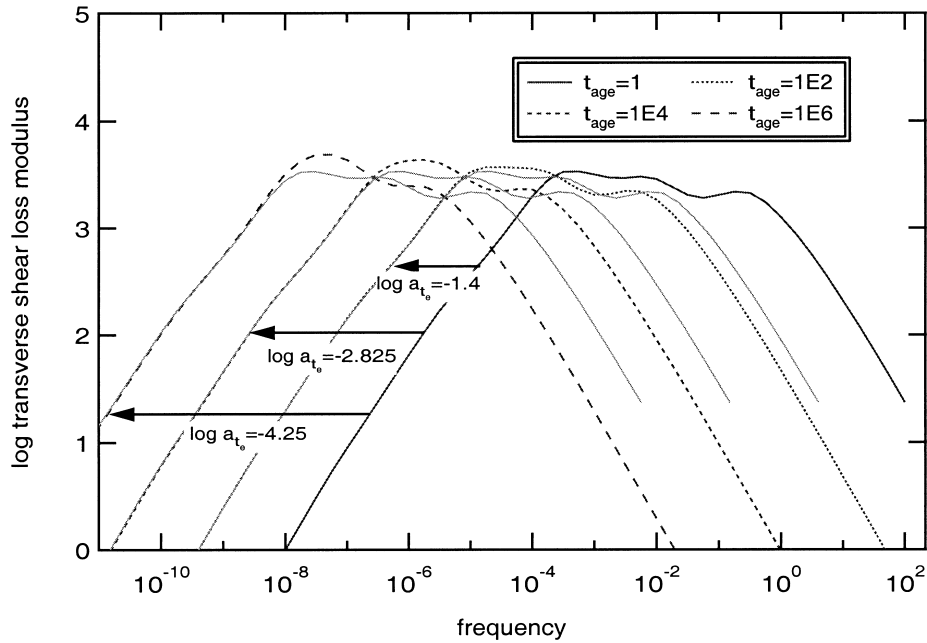


Fig. 14. Aged transverse shear loss moduli in the frequency domain for composite with 30% fiber, 10% soft interphase, 60% stiff matrix via FEA. Reference curve ($t_{\text{age}} = 1$) is shifted (shown as light gray lines) to the aged moduli such that low frequency data is matched.

do not overlap and thus prevent a unique shift factor from being determined. This type of behavior was found for all soft-interphase composites studied and is indicative of thermorheologically complex (TRC) behavior.

To circumvent this difficulty in shifting frequency domain moduli, the data were transformed into the time domain using a linear least squares solver [49]. Although the behavior of the material in the time domain is still TRC (see Fig. 15), the degree of mismatch between the moduli functions at different aging times is relatively small and, in practice, could easily be attributed to experimental scatter. If the slight non-overlap of the superposed curves in Fig. 15 is ignored, the results at different aging times can be shifted and a characteristic shift factor for the composite property determined.² These numerical tests in the time domain are then a reasonable model to ascertain if the interphase is responsible for the differences in shift rates seen experimentally. Thus, Eq. (15) was used to determine the effective shift rates as a function of composite configuration.

Table 3 shows shift rates calculated for different effective moduli via the FEA and the micromechanical solutions. The results suggest that the shift rates determined via FEA are largely dependent on the composite configuration. For composites where the interphase is the stiff

viscoelastic material, the shift rates μ_{22} and $\mu_{44} = \mu_{55}$ calculated using FEA are strongly dependent on the shift rate of the isotropic matrix. This is not the case when the interphase is the softest phase; here the overall shift rates of the composite are intermediate those of the viscoelastic phases (more evident for the 60% fiber case, where there is more interphase material per unit of matrix material). This suggests the influence of two separate factors which determine the effective physical aging of the composite: the shift rate of the softest VE material and the shift rate of the matrix phase. For stiff-interphase composites, both conditions suggest aging behavior dominated by the matrix, and in these instances the TRC behavior of the composite response is negligible. Similar results for other soft-interphase composite configurations support this hypothesis [43].

On the other hand, for soft-interphase composites, the shift rate of the matrix and the shift rate of the softest VE material (in this case the interphase) oppose each other, which may be responsible for the TRC behavior apparent in Fig. 14. This effect is magnified for larger fiber area fractions, as the ratio of the viscoelastic phases approaches unity. While TRC behavior has been seen in previous numerical studies of two-phase viscoelastic composites [20,25], the present work suggests that a relatively small area fraction of interphase can have a large role in determining the overall TRC behavior of the composite.

However, as the FEA results presented in Table 3 indicate, the interphase *does not* seem to cause a difference in the shift rates μ_{22} and $\mu_{44} = \mu_{55}$. Although this is circumstantial evidence (since the shift rate μ_{66} was not

² An important point illustrated by this analysis is that time domain data is much more forgiving than frequency domain data. Thermorheological complexity, which can invalidate time-temperature and time-aging time superposition, which may be masked in the time domain, may be more easily detected in the frequency domain.

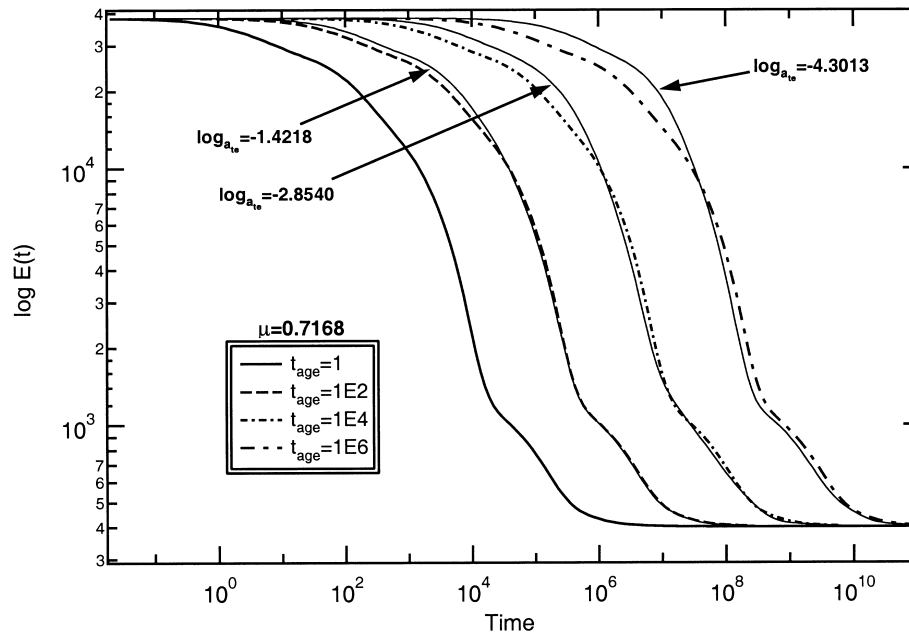


Fig. 15. Aged transverse Young’s moduli in the time domain for composite with 30% fiber, 10% soft interphase, 60% stiff matrix composite found via FEA. Reference curve ($t_{age}=1$) is shifted (shown as light gray lines) to the aged moduli.

Table 3

Effective shift rates found in the time domain for various composite configurations. Shift rates of the phase materials were $\mu_{mat}=0.70$ for the matrix and $\mu_{int}=0.85$ for the interphase

Method	Property	Geometry			
		30% fiber 10% stiff interphase 60% soft matrix	30% fiber 10% soft interphase 60% stiff matrix	60% fiber 10% stiff interphase 30% soft matrix	60% fiber 10% soft interphase 30% stiff matrix
FEA	μ_{22}	0.7003	0.7168	0.7003	0.7904
FEA	μ_{44}	0.6989	0.7144	0.6988	0.7847
BENV	μ_{22}	0.7007	0.8395	0.7006	0.8447
BENV	μ_{44}	0.7016	0.8421	0.7007	0.8461
BENV	μ_{66}	0.7011	0.7080	0.7008	0.7761
MT	μ_{22}	0.6989	0.7012	0.7011	0.7014
MT	μ_{44}	0.6997	0.7010	0.7000	0.7103
MT	μ_{66}	0.6987	0.7009	0.6988	0.6933

determined numerically in this work), these results suggest that *the interphase is not responsible for the difference in composite aging shift rates that is measured experimentally*. Although this should be verified by a 3D finite element analysis, these results imply that perhaps other mechanisms (e.g. residual stresses) cause polymeric composites to respond to physical aging differently than homogeneous polymer materials.

The shift rates determined via the micromechanical methods are also given in Table 3. In general, the solutions found using the Benveniste method are dominated by the softest VE phase in the composite, whereas the MT results are dictated by the shift rate of the matrix material. It is also interesting to note that the Benveniste

solution predicts a large difference in the transverse and axial shear shift rates, $\mu_{44}=\mu_{55}$ and μ_{66} , respectively, for the soft-interphase composite. While the Benveniste method was earlier demonstrated to have difficulties in predicting the effective moduli of composites with soft interphases, these results suggest that a full 3D FEA to analyze the interphase-dependence of the axial shear shift rate μ_{66} may be warranted.

7. Conclusions

This paper investigated the results of two micro-mechanical methods, the original Mori–Tanaka method

and an extension of the Mori–Tanaka model developed by Benveniste, for predicting the effective moduli of a three phase viscoelastic composite. The main conclusions of this work are outlined below:

- The micromechanical methods provide satisfactory approximations for the effective moduli in those cases where the matrix is the softest of the three phases. The difference between the MT and Benveniste solutions is minimal in these cases.
- When the interphase is the softest material, the integrity of the micromechanical methods is greatly diminished. Here the MT method is more effective in modeling the viscoelastic behavior of the composite because it predicts matrix-dominated effective moduli for the composite.
- For further work, it may be interesting to compare the methods used in this paper to a micromechanical analytic method with periodic unit cell arrangement, such as Aboudi's method of cells [50], although in general effective moduli have been shown to be independent of inclusion packing [31].
- The physical aging study indicated that thermorheologically complex behavior can be masked in time domain data, suggesting that frequency domain data may be preferred in order to identify TRC viscoelastic response. The loss modulus exhibits the greatest sensitivity to TRC behavior.
- The FEA results suggest that the interphase plays a large role in determining the overall shift rates of the composite. However, the interphase does *not* cause a difference in shift rates describing the physical aging of the transverse shear and axial shear moduli, μ_{22} and $\mu_{44} = \mu_{55}$, respectively. With this evidence, it seems unlikely that the interphase is responsible for the difference in μ_{22} and μ_{66} shift rates measured experimentally, although further verification with a 3D finite element analysis may be warranted.

Acknowledgements

The authors appreciate sponsorship from NSF for this work.

Appendix A. Transverse hydrostatic loading auxiliary problem for the Benveniste solution

Consider the single-inclusion auxiliary problem for the transverse hydrostatic loading shown as part of Fig. 3. Using standard elasticity theory [51] and the Correspondence Principle, the radial displacements in the transformed domain must take the following form,

$$\bar{u}_r^f = \bar{A}_f r, \quad \bar{u}_r^g = \bar{A}_g r + \frac{\bar{B}_g}{r}, \quad \bar{u}_r^m = \bar{A}_m r + \frac{\bar{B}_m}{r}, \quad (16)$$

where \bar{A}_i ($i=f,g,m$) and \bar{B}_j ($j=g,m$) are the unknown displacement constants, which are complex in nature. These constants are determined by requiring that the displacements satisfy suitable boundary conditions, including the far-field boundary conditions

$$\bar{\sigma}_{xx}|_{r \rightarrow \infty} = \bar{\sigma}_o, \quad \bar{\sigma}_{yy}|_{r \rightarrow \infty} = \bar{\sigma}_o. \quad (17)$$

The analysis then proceeds along the lines of a standard elasticity solution. Assuming a state of plane strain, the non-zero stresses in each isotropic phase can be written in terms of the complex Lamé and shear moduli, $\bar{\lambda}_i^*$ and \bar{G}_i^* , respectively,

$$\begin{aligned} \bar{\sigma}_{rr}^f &= 2 \bar{G}_f^* \bar{A}_f + \bar{\lambda}_f^* (2 \bar{A}_f) = 2 \bar{A}_f (\bar{G}_f^* + \bar{\lambda}_f^*) \\ \bar{\sigma}_{rr}^g &= 2 \bar{G}_g^* \left(\bar{A}_g - \frac{\bar{B}_g}{r^2} \right) + \bar{\lambda}_g^* (2 \bar{A}_g) \\ &= 2 \bar{A}_g (\bar{G}_g^* + \bar{\lambda}_g^*) - 2 \bar{G}_g^* \frac{\bar{B}_g}{r^2} \end{aligned} \quad (18)$$

$$\begin{aligned} \bar{\sigma}_{rr}^m &= 2 \bar{G}_m^* \left(\bar{A}_m - \frac{\bar{B}_m}{r^2} \right) + \bar{\lambda}_m^* (2 \bar{A}_m) \\ &= 2 \bar{A}_m (\bar{G}_m^* + \bar{\lambda}_m^*) - 2 \bar{G}_m^* \frac{\bar{B}_m}{r^2}, \end{aligned}$$

$$\begin{aligned} \bar{\sigma}_{\theta\theta}^f &= 2 \bar{G}_f^* \bar{A}_f + \bar{\lambda}_f^* (2 \bar{A}_f) = 2 \bar{A}_f (\bar{G}_f^* + \bar{\lambda}_f^*) \\ \bar{\sigma}_{\theta\theta}^g &= 2 \bar{G}_g^* \left(\bar{A}_g + \frac{\bar{B}_g}{r^2} \right) + \bar{\lambda}_g^* (2 \bar{A}_g) \\ &= 2 \bar{A}_g (\bar{G}_g^* + \bar{\lambda}_g^*) + 2 \bar{G}_g^* \frac{\bar{B}_g}{r^2} \end{aligned} \quad (19)$$

$$\begin{aligned} \bar{\sigma}_{\theta\theta}^m &= 2 \bar{G}_m^* \left(\bar{A}_m + \frac{\bar{B}_m}{r^2} \right) + \bar{\lambda}_m^* (2 \bar{A}_m) \\ &= 2 \bar{A}_m (\bar{G}_m^* + \bar{\lambda}_m^*) + 2 \bar{G}_m^* \frac{\bar{B}_m}{r^2}. \end{aligned}$$

Enforcing the boundary conditions provides the following five simultaneous equations, from which the unknown displacement constants can be determined,

$$\begin{aligned} \bar{A}_f a &= \bar{A}_g a + \frac{\bar{B}_g}{a} \\ \bar{A}_g b + \frac{\bar{B}_g}{b} &= \bar{A}_m b + \frac{\bar{B}_m}{b} \end{aligned}$$

$$\begin{aligned}
 2 \bar{A}_f(\bar{G}_f^* + \bar{\lambda}_f^*) &= 2 \bar{A}_g(\bar{G}_g^* + \bar{\lambda}_g^*) - 2 \bar{G}_g^* \frac{\bar{B}_g}{a^2} \\
 2 \bar{A}_g(\bar{G}_g^* + \bar{\lambda}_g^*) - 2 \bar{G}_g^* \frac{\bar{B}_g}{b^2} &= 2 \bar{A}_m(\bar{G}_m^* + \bar{\lambda}_m^*) - 2 \bar{G}_m^* \frac{\bar{B}_m}{b^2} \\
 2 \bar{A}_m(\bar{G}_m^* + \bar{\lambda}_m^*) &= \bar{\sigma}_o,
 \end{aligned} \tag{20}$$

where a and b are the outer radius of the fiber and the interphase, respectively.

Given these displacement constants, one can now solve for the phase average stresses in the fiber and interphase ($k=f,g$) using the relationship

$$\tilde{\sigma}_{ij}^k = \frac{\int_0^{2\pi} \int_{r_i}^{r_o} \bar{\sigma}_{ij}^k \cdot r \, dr \, d\theta}{\pi(r_o^2 - r_i^2)}. \tag{21}$$

Note that phase-averaged quantities are denoted by $(\bar{\bullet})$. Following the work of Benveniste [24], we now define scalar stress concentration factors \bar{W}_{ij}^k which relate the applied far-field stress of the auxiliary problem to the corresponding phase-averaged stresses in the included phases ($k=f,g$),

$$\begin{aligned}
 \tilde{\sigma}_{xx}^k &= \bar{W}_{XX}^k \bar{\sigma}_o, \quad \tilde{\sigma}_{yy}^k = \bar{W}_{YY}^k \bar{\sigma}_o, \\
 \tilde{\sigma}_{zz}^k &= \bar{W}_{ZZ}^k \bar{\sigma}_o = 2 \bar{v}_k^* \bar{W}_{XX}^k \bar{\sigma}_o,
 \end{aligned} \tag{22}$$

where \bar{v}_k^* is the complex Poisson ratio of the k th phase. Note that due to symmetry, \bar{W}_{XX}^k and \bar{W}_{YY}^k are identical. These stress concentration factors can be written explicitly as

$$\bar{W}_{XX}^f = \frac{2 \bar{A}_f}{\bar{\sigma}_o} (\bar{G}_f^* + \bar{\lambda}_f^*), \quad \bar{W}_{ZZ}^f = \frac{2 \bar{A}_f \bar{\lambda}_f^*}{\bar{\sigma}_o}, \tag{23}$$

$$\bar{W}_{XX}^g = \frac{2 \bar{A}_g}{\bar{\sigma}_o} (\bar{G}_g^* + \bar{\lambda}_g^*), \quad \bar{W}_{ZZ}^g = \frac{2 \bar{A}_g \bar{\lambda}_g^*}{\bar{\sigma}_o}. \tag{24}$$

Appendix B. Transverse shear loading auxiliary problem for the Benveniste solution

Consider the single-inclusion auxiliary problem for the transverse shear loading, the second of the two auxiliary problems shown in Fig. 3. The displacements for this problem can be written [52] as follows,

$$\begin{aligned}
 \bar{u}_r^f &= \left(\frac{b \bar{\sigma}_o}{4 \bar{G}_f^*} \right) \left\{ \bar{a}_1 (\bar{\eta}_f^* - 3) \left(\frac{r}{b} \right)^3 + \bar{d}_1 \left(\frac{r}{b} \right) \right\} \cos 2\theta \\
 \bar{u}_\theta^f &= \left(\frac{b \bar{\sigma}_o}{4 \bar{G}_f^*} \right) \left\{ \bar{a}_1 (\bar{\eta}_f^* + 3) \left(\frac{r}{b} \right)^3 - \bar{d}_1 \left(\frac{r}{b} \right) \right\} \sin 2\theta,
 \end{aligned} \tag{25}$$

$$\begin{aligned}
 \bar{u}_r^g &= \left(\frac{b \bar{\sigma}_o}{4 \bar{G}_g^*} \right) \left\{ \bar{a}_2 (\bar{\eta}_g^* - 3) \left(\frac{r}{b} \right)^3 + \bar{d}_2 \left(\frac{r}{b} \right) + \bar{c}_2 (\bar{\eta}_g^* + 1) \left(\frac{b}{r} \right) \right. \\
 &\quad \left. + \bar{b}_2 \left(\frac{b}{r} \right)^3 \right\} \cos 2\theta
 \end{aligned}$$

$a \leq r \leq b$,

$$\begin{aligned}
 \bar{u}_\theta^g &= \left(\frac{b \bar{\sigma}_o}{4 \bar{G}_g^*} \right) \left\{ \bar{a}_2 (\bar{\eta}_g^* + 3) \left(\frac{r}{b} \right)^3 - \bar{d}_2 \left(\frac{r}{b} \right) - \bar{c}_2 (\bar{\eta}_g^* - 1) \left(\frac{b}{r} \right) \right. \\
 &\quad \left. + \bar{b}_2 \left(\frac{b}{r} \right)^3 \right\} \sin 2\theta,
 \end{aligned} \tag{26}$$

$$\begin{aligned}
 \bar{u}_r^m &= \left(\frac{b \bar{\sigma}_o}{4 \bar{G}_m^*} \right) \left\{ 2 \left(\frac{r}{b} \right) + (\bar{\eta}_m^* + 1) \bar{a}_3 \left(\frac{b}{r} \right) + \bar{c}_3 \left(\frac{b}{r} \right)^3 \right\} \cos 2\theta \\
 \bar{u}_\theta^m &= \left(\frac{b \bar{\sigma}_o}{4 \bar{G}_m^*} \right) \left\{ -2 \left(\frac{r}{b} \right) - (\bar{\eta}_m^* - 1) \bar{a}_3 \left(\frac{b}{r} \right) + \bar{c}_3 \left(\frac{b}{r} \right)^3 \right\} \sin 2\theta,
 \end{aligned} \tag{27}$$

where $\bar{\eta}_k^* = 3 - 4 \bar{v}_k^*$ and all other displacements are equal to zero.

These displacement equations contain 8 unknown constants, which again can be complex in nature. These constants are determined using the set of simultaneous equations given below, where $\alpha = b/a$:

$$\begin{aligned}
 \bar{G}_g^* [\bar{a}_1 (\bar{\eta}_f^* - 3) + \bar{d}_1 \alpha^2] &= \bar{G}_f^* [\bar{a}_2 (\bar{\eta}_g^* - 3) \\
 &\quad + \bar{d}_2 \alpha^2 + \bar{c}_2 (\bar{\eta}_g^* + 1) \alpha^4 + \bar{b}_2 \alpha^6] \\
 \bar{G}_g^* [\bar{a}_1 (\bar{\eta}_f^* + 3) - \bar{d}_1 \alpha^2] &= \bar{G}_f^* [\bar{a}_2 (\bar{\eta}_g^* + 3) \\
 &\quad - \bar{d}_2 \alpha^2 - \bar{c}_2 (\bar{\eta}_g^* - 1) \alpha^4 + \bar{b}_2 \alpha^6] \\
 \bar{G}_m^* [\bar{a}_2 (\bar{\eta}_g^* - 3) + \bar{d}_2 + \bar{c}_2 (\bar{\eta}_g^* + 1) + \bar{b}_2] \\
 &= \bar{G}_g^* [2 + \bar{a}_3 (\bar{\eta}_m^* + 1) + \bar{c}_3] \\
 \bar{G}_m^* [\bar{a}_2 (\bar{\eta}_g^* + 3) - \bar{d}_2 - \bar{c}_2 (\bar{\eta}_g^* - 1) + \bar{b}_2] \\
 &= \bar{G}_g^* [-2 - \bar{a}_3 (\bar{\eta}_m^* - 1) + \bar{c}_3] \\
 2 \bar{G}_g^* \bar{G}_f^* \{ 3 \bar{a}_1 (\bar{\eta}_f^* - 3) + \bar{d}_1 \alpha^2 \} + \bar{G}_g^* \bar{\lambda}_f^* \{ 6 \bar{a}_1 (\bar{\eta}_f^* - 1) \} &= 2 \bar{G}_g^* \bar{G}_f^* \\
 * \{ 3 \bar{a}_2 (\bar{\eta}_g^* - 3) + \bar{d}_2 \alpha^2 - \bar{c}_2 (\bar{\eta}_g^* + 1) \alpha^4 - 3 \bar{b}_2 \alpha^6 \} \\
 + \bar{G}_f^* \bar{\lambda}_g^* \{ 6 \bar{a}_2 (\bar{\eta}_g^* - 1) - 2 \bar{c}_2 (\bar{\eta}_g^* - 1) \alpha^4 \} \\
 6 \bar{a}_1 - \bar{d}_1 \alpha^2 &= 6 \bar{a}_2 - \bar{d}_2 \alpha^2 - 2 \bar{c}_2 \alpha^4 - 3 \bar{b}_2 \alpha^6 \\
 2 \bar{G}_m^* \bar{G}_g^* \{ 3 \bar{a}_2 (\bar{\eta}_g^* - 3) + \bar{d}_2 - \bar{c}_2 (\bar{\eta}_g^* + 1) - 3 \bar{b}_2 \} \\
 + \bar{G}_m^* \bar{\lambda}_g^* \{ 6 \bar{a}_2 (\bar{\eta}_g^* - 1) - 2 \bar{c}_2 (\bar{\eta}_g^* - 1) \} \\
 &= 2 \bar{G}_m^* \bar{G}_g^* \{ 2 - \bar{a}_3 (\bar{\eta}_m^* + 1) - 3 \bar{c}_3 \} + \bar{G}_g^* \bar{\lambda}_m^* \{ 2 \bar{a}_3 (1 - \bar{\eta}_m^*) \} \\
 6 \bar{a}_2 - \bar{d}_2 - 2 \bar{c}_2 - 3 \bar{b}_2 &= -2 - 2 \bar{a}_3 - 3 \bar{c}_3.
 \end{aligned} \tag{28}$$

Following the procedure outlined in the previous section, stress concentration factors \bar{W}_{TS}^k are defined relating the phase-averaged stress in the included phases to the applied far-field stress in the auxiliary problem, such that

$$\tilde{\sigma}_{xx}^k = -\bar{W}_{TS}^k \bar{\sigma}_o, \quad \tilde{\sigma}_{yy}^k = \bar{W}_{TS}^k \bar{\sigma}_o. \quad k = \{f, g\} \quad (29)$$

After algebraic manipulation, these factors can be simplified as

$$\begin{aligned} \bar{W}_{TS}^f &= -\frac{3\bar{a}_1 a^2}{2b^2} + \frac{\bar{d}_1}{2} \\ \bar{W}_{TS}^g &= -\frac{3\bar{a}_2(b^2 + a^2)}{2b^2} + \frac{\bar{d}_2}{2}. \end{aligned} \quad (30)$$

Appendix C. Effective transverse Young's modulus of the composite via Benveniste solution

Having analyzed the previous two auxiliary problems, we are now in a position to superpose the solutions to determine the effective transverse Young's modulus of the composite. The procedure to determine the transverse shear modulus is similar and will not be covered here. We first assume that the stress concentration factors \bar{W}_{ij}^k , which were calculated using the single-inclusion auxiliary problem, are sufficient to use for the multiple-inclusion composite. In addition, we assume that for the actual composite, the far-field stress to which each inclusion is subjected is the unknown average stress in the matrix, which for the current loading mode is $\tilde{\sigma}_{yy}^m$.

Using the stress-concentration factors derived previously, the average stress components in the fiber and interphase regions of the composite can be written in terms of this unknown stress,

$$\begin{aligned} \tilde{\sigma}_{yy}^k &= (\bar{W}_{XX}^k + \bar{W}_{TS}^k) \tilde{\sigma}_{yy}^m, \\ \tilde{\sigma}_{xx}^k &= (\bar{W}_{XX}^k - \bar{W}_{TS}^k) \tilde{\sigma}_{yy}^m, \\ \tilde{\sigma}_{zz}^k &= \bar{W}_{LT}^k \tilde{\sigma}_{yy}^m. \end{aligned} \quad (31)$$

Enforcing that the sum of the average phase stresses in the y -direction must equal the applied far-field stress, in this case $2\bar{\sigma}_o$, yields

$$\begin{aligned} 2\bar{\sigma}_o &= \sum_k c_k \tilde{\sigma}_{yy}^k = c_m \tilde{\sigma}_{yy}^m + c_f \tilde{\sigma}_{yy}^f + c_g \tilde{\sigma}_{yy}^g \\ &= c_m \tilde{\sigma}_{yy}^m + c_f (\bar{W}_{XX}^f + \bar{W}_{TS}^f) \tilde{\sigma}_{yy}^m \\ &\quad + c_g (\bar{W}_{XX}^g + \bar{W}_{TS}^g) \tilde{\sigma}_{yy}^m, \end{aligned} \quad (32)$$

where c_f and c_g are the normalized areas of the included phases, and $c_m = 1 - c_f - c_g$. Thus the average y -component of the matrix stress can be found,

$$\tilde{\sigma}_{yy}^m = \frac{2\bar{\sigma}_o}{c_m + c_f (\bar{W}_{XX}^f + \bar{W}_{TS}^f) + c_g (\bar{W}_{XX}^g + \bar{W}_{TS}^g)}. \quad (33)$$

Likewise, other average stress components in the matrix can be determined. Once this is completed, we are in a position to evaluate the transverse Young's modulus of the composite, as shown in Fig. 2. Consider the expression

$$\bar{\varepsilon}_{yy} = \frac{\bar{\sigma}_{yy}}{E_{22}^*} = \sum_k c_k \tilde{\varepsilon}_{yy}^k, \quad (34)$$

where $\bar{\varepsilon}_{yy}$ is the overall composite strain in the y -direction, $\bar{\sigma}_{yy}$ is the applied far-field stress in the same direction, and E_{22}^* is the effective transverse Young's modulus of the composite. For the superposition problem considered here, we have

$$\frac{2\bar{\sigma}_o}{E_{22}^*} = c_f \tilde{\varepsilon}_{yy}^f + c_g \tilde{\varepsilon}_{yy}^g + c_m \tilde{\varepsilon}_{yy}^m. \quad (35)$$

Since all phase average stresses can now be determined, the average strain in the phases can be found using Hooke's Law,

$$\tilde{\varepsilon}_{yy}^k = \frac{1}{2\bar{G}_k^*} \left\{ \tilde{\sigma}_{yy}^k - \bar{\nu}_k^* (\tilde{\sigma}_{xx}^k + \tilde{\sigma}_{yy}^k + \tilde{\sigma}_{zz}^k) \right\}. \quad k = \{f, g, m\} \quad (36)$$

Substitution into (35) allows the numerical calculation of the transverse Young's modulus of the composite. This expression is too unwieldy to present in its algebraic form.

As a final note, the stress-concentration scalars defined in (30) can be used to calculate the effective transverse shear modulus, \bar{G}_{44}^* , of the composite. Again following the procedure of [24], the transverse shear modulus of the composite is found to be,

$$\frac{1}{2\bar{G}_{44}^*} = \frac{c_m \frac{1}{2\bar{G}_m^*} + c_f \frac{1}{2\bar{G}_f^*} \bar{W}_{TS}^f + c_g \frac{1}{2\bar{G}_g^*} \bar{W}_{TS}^g}{c_m + c_f \bar{W}_{TS}^f + c_g \bar{W}_{TS}^g}. \quad (37)$$

Appendix D. Effective axial shear modulus of the composite via Benveniste solution

The solution for the axial shear auxiliary problem follows an identical procedure. Suitable displacement equations for this problem are as follows,

$$\begin{aligned} \bar{u}_z^f &= \bar{A}_f r \sin\theta, & \bar{u}_z^g &= \left(\bar{A}_g r + \frac{\bar{B}_g}{r} \right) \sin\theta, \\ \bar{u}_z^m &= \left(\bar{A}_m r + \frac{\bar{B}_m}{r} \right) \sin\theta. \end{aligned} \quad (38)$$

By defining the appropriate stress concentration factors for the included phases as

$$\bar{\sigma}_{yz}^k = \bar{W}_{LS}^k \bar{\sigma}_o, \quad (39)$$

where $\bar{\sigma}_{yz}^k = \bar{\sigma}_{rz}^k \sin\theta + \bar{\sigma}_{\theta z}^k \cos\theta$, one can find these factors to be equal to

$$\bar{W}_{LS}^f = \frac{\bar{G}_f^* \bar{A}_f}{\bar{\sigma}_o}, \quad \bar{W}_{LS}^g = \frac{\bar{G}_g^* \bar{A}_g}{\bar{\sigma}_o}. \quad (40)$$

Solving for the unknown average matrix stress for the actual geometry as

$$\bar{\sigma}_{yz}^m = \frac{\bar{\sigma}_o}{c_m + c_f \bar{W}_{LS}^f + c_g \bar{W}_{LS}^g}, \quad (41)$$

one can use the following expression for the effective axial shear modulus of the composite,

$$\bar{G}_{66}^* = \frac{c_m + c_f \bar{W}_{LS}^f + c_g \bar{W}_{LS}^g}{\frac{c_m}{\bar{G}_m^*} + \frac{c_f \bar{W}_{LS}^f}{\bar{G}_f^*} + \frac{c_g \bar{W}_{LS}^g}{\bar{G}_g^*}}. \quad (42)$$

References

[1] Thomason JL. The interface region in glass fibre-reinforced epoxy resin composites: 3. Characterization of fibre surface coatings and the interphase. *Composites* 1995;26:487–98.

[2] Hashin Z. Analysis of composite materials — a survey. *Journal of Applied Mechanics* 1983;50:481–505.

[3] Christensen RM. A critical evaluation for a class of micro-mechanics models. *Journal of the Mechanics and Physics of Solids* 1990;38(3):379–404.

[4] Zhao YH, Weng GJ. Effective elastic moduli of ribbon-reinforced composites. *Journal of Applied Mechanics* 1990;57:158–67.

[5] Chen T, Dvorak GJ, Benveniste Y. Mori-Tanaka estimates of the overall elastic moduli of certain composite materials. *Journal of Applied Mechanics* 1992;59:539–46.

[6] Qui YP, Weng GJ. The influence of inclusion shape on the overall elastoplastic behavior of a two-phase isotropic composite. *International Journal of Solids and Structures* 1991;27(12):1537–50.

[7] Avery WB, Herakovich CT. Effect of fiber anisotropy on thermal stresses in fibrous composites. *Journal of Applied Mechanics* 1986;53:751–6.

[8] Mikata Y. Stress fields in a continuous fiber composite with a variable interphase under thermo-mechanical loadings. *Journal of Engineering Materials and Technology* 1994;116:367–77.

[9] Qui YP, Weng GJ. Elastic moduli of thickly coated particle and fiber-reinforced composites. *Journal of Applied Mechanics* 1991;58:388–98.

[10] Weng GJ. The theoretical connection between Mori–Tanaka’s theory and the Hashin–Shtrikman–Wadpole bounds. *International Journal of Engineering Science* 1990;28(11):1111–20.

[11] Hashin Z. Viscoelastic behavior of heterogeneous media. *Journal of Applied Mechanics* 1965;32:630–6.

[12] Hashin Z. Viscoelastic fiber reinforced materials. *AIAA Journal* 1966;4:1411–7.

[13] Hashin Z. Complex moduli of viscoelastic composites: II. Fiber reinforced materials. *International Journal of Solids and Structures* 1970;6:797–807.

[14] Hashin Z. Complex moduli of viscoelastic composites: I. General theory and application to particulate composites. *International Journal of Solids and Structures* 1970;6:539–52.

[15] Schapery RA. On the characterization of nonlinear viscoelastic materials. *Polymer Engineering and Science* 1969;9(4):295–310.

[16] Schapery RA. Stress analysis of composite materials. *Journal of Composite Materials* 1967;1:228–67.

[17] Wang YM, Weng GJ. The influence of inclusion shape on the overall viscoelastic behavior of composites. *Journal of Applied Mechanics* 1992;59:510–8.

[18] Li J, Weng GJ. Effective creep behavior and complex moduli of fiber and ribbon-reinforced polymer–matrix composites. *Composites Science and Technology* 1994;52:615–29.

[19] Brinson LC, Lin WS. Comparison of micromechanics methods for effective properties of multiphase viscoelastic composites. *Composite Structures* 1998;41(3-4):353–67.

[20] Lin WSA. comparison of finite element analysis and Mori–Tanaka theorem for the transverse behavior of two phase viscoelastic composites. Northwestern University, 1996.

[21] Mori T, Tanaka K. Average stress in matrix and average elastic energy of materials with misfitting inclusions. *Acta Metallurgica* 1973;21:571–4.

[22] Weng GJ. Some elastic properties of reinforced solids, with special reference to isotropic ones containing spherical inclusions. *International Journal of Engineering Science* 1984;22(7):845–56.

[23] Benveniste Y. A new approach to the application of Mori–Tanaka’s theory in composite materials. *Mechanics of Materials* 1987;6:147–57.

[24] Benveniste Y, Dvorak GJ, Chen T. Stress fields in composites with coated inclusions. *Mechanics of Materials* 1989;7:305–17.

[25] Brinson LC, Knauss WG. Finite element analysis of multiphase viscoelastic solids. *Journal of Applied Mechanics* 1992;59:730–7.

[26] Achenbach J, Zhu H. Effect of interphases on micro and macro-mechanical behavior of hexagonal-array fiber composites. *Journal of Applied Mechanics* 1990;57(4):956–63.

[27] Gosz M, Moran B, Achenbach J. Effect of a viscoelastic interface on the transverse behavior of fiber-reinforced composites. *International Journal of Solids and Structures* 1991;27(14):1757–71.

[28] Hashin Z. Extremum-principles for elastic heterogenous media with imperfect interfaces and their application to bounding of effective moduli. *Journal of the Mechanics and Physics of Solids* 1992;40(4):767–81.

[29] Broutman LJ, Agarwal BD. A theoretical study of the effect of an interfacial layer on the properties of composites. *Polymer Engineering and Science* 1974;14(8):581–8.

[30] Wacker G, Bledzki AK, Chate A. Effect of interphase on the transverse Young’s modulus of glass/epoxy composites. *Composites Part A* 1998;29A:619–26.

[31] Al-Ostaz A, Jasiuk I. The influence of interface and arrangement of inclusions on local stresses in composite materials. *Acta Metallurgica* 1996;45(10):4131–43.

[32] Yi S, et al. Effective transverse modulus of composites with viscoelastic interphase. *AIAA Journal* 1995;33(8):1548–50.

- [33] Fink BK, McCullough RL. Interphase research issues. *Composites Part A* 1999;30(1):1–2.
- [34] Gardner SD, Pittman CU Jr, Hackett RM. Residual thermal stresses in filamentary polymer–matrix composites containing an elastomeric interphase. *Journal of Composite Materials* 1993;27(8):830–60.
- [35] Papanicolaou GC, Messinis GJ, Karakatsanidis SS. The effect of interfacial conditions on the elastic-longitudinal modulus of fibre reinforced composites. *Journal of Materials Science* 1989;24:395–401.
- [36] Theocaris PS. The unfolding model for the representation of the mesophase layer in composites. *Journal of Applied Polymer Science* 1985;30:621–45.
- [37] Termonia Y. Fibre coating as a means to compensate for poor adhesion in fibre-reinforced materials. *Journal of Materials Science* 1990;25:103–6.
- [38] Munz M, et al. The scanning force microscope as a tool for the detection of local mechanical properties within the interphase of fibre reinforced polymers. *Composites Part A* 1998;29A:1251–9.
- [39] Mai K, Mader E, Muhle M. Interphase characterization in composites with new non-destructive methods. *Composites Part A* 1998;29A:1111–9.
- [40] VanLandingham MR, et al. Characterization of nanoscale property variations in polymer composite systems: 1. Experimental results. *Composites Part A* 1999;30(1):75–83.
- [41] Ferry JD. *Viscoelastic properties of polymers*. 3rd ed. New York: John Wiley & Sons, 1980 p. 641.
- [42] Brinson LC, Knauss WG. Thermorheologically complex behavior of multi-phase viscoelastic materials. *Journal of the Mechanics and Physics of Solids* 1991;39(7):859–80.
- [43] Fisher, F.T., *Viscoelastic behavior of polymer matrix composites with interphase effects: theoretical models and finite element analysis*, Northwestern University, 1998.
- [44] Gibiansky LV, Milton GW. On the effective viscoelastic moduli of two-phase media. I. Rigorous bounds on the complex-bulk modulus. *Proceedings of the Royal Society of London A* 1993;440:163–88.
- [45] Gibiansky LV, Lakes R. Bounds on the complex bulk modulus of a two-phase viscoelastic composite with arbitrary volume fractions of the components. *Mechanics of Materials* 1993;16:317–31.
- [46] Struik LCE. *Physical aging in amorphous polymers and other materials*. New York: Elsevier, 1978.
- [47] Gates TS, Feldman M. Time dependent behavior of a graphite/thermoplastic composite and the effects of stress and physical aging, 1993, NASA Technical Memorandum.
- [48] Hastie RLJ, Morris DH. The effects of physical aging on the creep response of a thermoplastic composite. In: Harris C., Gates T., editors. *High temperature and environmental effects in polymer matrix composites*. Philadelphia: ASTM STP 1174, 1993. p. 163–85.
- [49] Bradshaw RD, Brinson LC. A sign control method for fitting and interconverting material functions for linearly viscoelastic materials. *Mechanics of Time-Dependent Materials* 1997;1:85–108.
- [50] Aboudi J. *Mechanics of composite materials — a unified micro-mechanics approach*. Amsterdam: Elsevier, 1991 p. 328.
- [51] Timoshenko SP, Goodier JN. *Theory of Elasticity*. 3rd ed. New York: McGraw-Hill, 1970 p. 567.
- [52] Christensen RM, Lo KH. Solutions for effective shear properties in three phase sphere and cylinder models. *Journal of the Mechanics and Physics of Solids* 1979;27:315.